Assisted gait phase estimation through an embedded depth camera using modified Random Forest algorithm classification

Simone Pasinetti, Alberto Fornaser, Matteo Lancini, Mariolino De Cecco, and Giovanna Sansoni

***Abstract*—The paper presents a novel method for the classification of gait phases for power gait orthosis users based on machine learning. The classification uses depth images collected from a Time of Flight camera embedded in the crutches employed for the assisted gait. The machine learning algorithm foresees an initial phase of data collection and processing, identifying the 3D points belonging to the foot and those belonging to the floor. From these, a feature set is computed analyzing the values of percentiles of distances of the foot from the floor, and passed to a modified version of Random Forest classifier, called Sigma-z Random Forest. The classifier considers the uncertainties associated to each feature set and provides both the classification of the gait phase (stance or swing) and an associated confidence value. In this work, we propose the use of the confidence value to improve the reliability of the gait phase classification, by applying an optimized threshold to the confidence value obtained for each new frame. The algorithm has been tested on different subjects and environments. An average classification accuracy of 87.3% has been obtained (+6.3% with respect to the standard random forest classifier), with a minor loss of unclassifiable frames. Results highlight that unclassifiable samples are usually associated to transitions between stance and swing.**

***Index Terms*—Depth sensing; measurement, uncertainty, gait analysis, classification.**

I. Introduction

THE loss of locomotion is one of the major impairments that could result from a spinal cord injury. Advancements in medical treatments could lead to increase the quality of life in patients affects by spinal cord injury. These patients, however, are easily affected by secondary pathologies related to the use of wheelchairs as primary means of locomotion, and to the loss of the erect position. To overcome such limitations, in recent years, novel active orthosis (often called exoskeletons) have been developed [1]–[3]. Different studies show their efficacy in terms of medical effects as well as social interactions [2], [4], [5].

Unfortunately, most of these studies are performed in medical environments, such as hospitals or specialized gait labs, where motion capture systems, force platforms and other sensors are used to define the full kinematic model of the patients [6], [7]. These studies are limited to indoor applications, with short paths walked per session and with the continuous presence of the medical staff. A further drawback is that the behavior of a patient during an assisted walking session is strongly influenced by the type of environment [8].

To overcome the highlighted issues, a set of wireless forearm instrumented crutches were developed in past works [9]–[11]. The crutches are instrumented with IMUs and strain gauges to measure their orientation and the axial forces exerted by the user on them. Data acquired with the developed crutches, together with the definition of a kinematic model of the user, allow the measurement of upper limbs involvement during assisted gait in a more natural setting, and without relying on the exoskeleton specific model, or capabilities. These, however, still rely on the gait lab motion capture system to relate the measured forces to the gait phases.

We solved this limitation by modifying the aforementioned instrumented crutches by adding two compact Time-Of-Flight (TOF) cameras (PMD^{TM} Camboard Picoflexx) for the acquisition of the controlateral foot. In the proposed strategy, the first step is the extraction of the features from the depth images, achieved by segmenting the 3D point cloud into the user foot and the floor. In the second step, the classification of the gait phases (stance and swing phases) is achieved through machine learning techniques, that classify collected frames. The Random Forest (RF) algorithm has been selected as the most appropriate for our application, since it represents a good trade-off between simplicity and accuracy of the classification [12]. The input entries are M=15 suitable features assigned to each acquired frame, and the training phase of the classifier is performed using the classical, well known RF approach; instead, the classification of new point clouds is accomplished using a modified version of the RF algorithm, previously developed by some of the authors. This algorithm, extensively presented in [13], aims at improving the robustness of the classification by assessing a confidence level of the classification, expressed as the probability that the identified class (i.e., swing or stance) is not confused with the other, even when the input data sets are characterized by uncertainty levels and population variances which could result in wrong classifications. This algorithm is called *Sigma-z Random Forest*: it provides a statistical inferential approach by considering both the uncertainty of a new input feature and the variance of the distribution of the training set. These elements are combined into the classical RF method, and allow the evaluation of a parameter, there after called *classification confidence* that indicates which class presents the highest probability of being the correct one. The gait classification output is then synchronized with the force sensors to refer the

S. Pasinetti, M. Lancini and G. Sansoni are with the Department of Mechanical and Industrial Engineering, University of Brescia, Brescia, Italy e-mail: simone.pasinetti@unibs.it

A. Fornaser and M. De Cecco are with the Department of Industrial Engineering, University of Trento, Italy

dynamic measurements (forces exerted by the user) to the user kinematics (state of each foot).

In this paper, we present the results of the experimentation carried out considering four expert users wearing a Rewalk™ exoskeleton (Argo Medical Technologies Ltd., Yokneam Ilit, Israel) during different walking sessions. The classification algorithm has been trained using the initial gait performed by each user to take into account the variability of the subjects gait style and clothes; additional gaits were then performed by each user for testing the algorithm performances.

The paper is organized as follows: Section II presents a review of the literature regarding gait analysis methods, Section III describes the system set-up. Section IV presents the approach to the extraction of the features and the gait phase classification method using the Sigma-z RF classifier. Section V reports the results of the experiments and demonstrates the validity of the chosen approach.

II. State of the art of gait analysis methods

One of the main indeces of performances of exoskeleton users is the quality of gait. An excellent technique to assess this parameter is the detection of gait events, such as heel contact and toe off, to divide the gait in swing and stance phases.

Gait analysis is commonly performed using motion capture systems based on inertial sensors [14]–[21] or cameras [22]–[29]. Among the latter, many studies use Time-Of-Flight (TOF) cameras to acquire 3D point clouds of the scene through depth images.

TOF cameras represent an emerging technology for three-dimensional measurements: these devices measure the distance of each point of the scene by measuring the TOF of a signal sent by an emitter (placed inside the camera) and reflected back by the objects in the scene. In [30], a single fixed TOF camera is used to extract the silhouette of the walking subject using segmentation algorithms. The gait phases are assessed from joint angles resulting from the analysis of the silhouette. Works [31], [32] exploit a combination of intensity images and depth images, both acquired with the same TOF camera. In [31], a number of markers are placed on the walking subject and the joint and body segments positions are extracted selecting the markers from the intensity images, and their respective 3D coordinates from the depth images. In [32], a Markov Random Field is used to fit an articulated model of the walker, while in [33], a comparison between a wearable inertial system and a structured light video system is performed for the estimation of the gait parameters. In these studies, the camera is placed in a fixed position in the environment. This solution suffers from some disadvantages: a limited field of view, a limited depth range, and the need of a custom environment (specifically organized for the analysis).

These limitations could be overcome using moving cameras (RGB or TOF based) instead of fixed ones. In the literature, two different approaches have been developed: in the former, the camera is attached directly at the walking subject; in the latter, the camera is placed on a walking device, moved by the subject or autonomously.

As for the first approach, wearable solutions have been implemented to measure the gait parameters. In [34], a single RGB camera is mounted (pointing downward) on the leg of the walking subject. In [35], the gait parameters are measured using a smart-phone camera attached to the hip of the subject using a waist bell. The camera recognizes the feet using two colored markers directly attached to the dorsum of the feet. In [36], a system consisting of an RGB camera, eight LED markers and a single board computer is presented. The system is mounted on each shoe of the subject, and the gait parameters are measured analyzing the markers detected in images acquired by two cameras. In [37], a camera is embedded into a pair of glasses. The gait parameters are measured extracting the motion vectors of the scene. In these wearable solutions, the sensors are mounted directly on the user and the approach requires a setup phase very time consuming. Furthermore, the wearable solutions could be stressful, especially for exoskeleton users. Both represent not negligible limitations.

In the second approach, different kind of supports are used to move the camera. In [38] and [39] for example, a RGB camera is mounted on instrumented rollators moved by healthy subjects. The camera captures the feet of the subject during the locomotion, and estimates the step width from the video data. In [40], two Kinect sensors are installed on a moving device. A set of algorithms has been developed to extract anatomical data. These are used in a physical model of a virtual human to reproduce and analyze the observed motion. In [41], a combination of a wearable sensor and a depth vision sensor is used for gait analysis. The wearable sensor captures the head motion while the vision sensor captures color and depth information of the scene. To increase the measurement range, the vision sensor is mounted onto a mobile robot which follows the subject during his/her motion through human tracking algorithms. The limitations of these studies are principally related to the type of support, which is completely dedicated to the camera placement.

Considerable work has been done to integrate the traditional foot switch and pressure-based sensors with a segmentation approach, to compensate for the low reliability of these devices in long walks, as in [42] and in [43]. However, foot switches and pressure-based sensors can be difficult to adapt to exoskeleton pilots. In the case of exoskeleton users, some approaches have been focused on force and angular sensors already available onboard the robot, as in [44]–[46], but these techniques depend on the availability of these sensors on the robot. Publication [47] presents a comparison between different alghorithms to extract gait phases from inertial units worn by the subject and surface electromyography, while [48] presents inertial units and an adaptive Bayesian approach for recognition of walking activities. Reference [49] presents instead a classification method based on a single 3D depth camera and 12 key feature, to provide a reliable and low cost way to assess the gait phases. All the sensors used in these works, however, are either worn by the user, or monitor a limited volume of space where the user can walk.

In our work, the acquisition sensors are not mounted on the user neither constrained to a limited walking space; instead,

they are mounted directly on the instrumented crutches, which are part of the rehabilitation setup and mandatory during the user gait.

Among classification methods, very few references are available on the topic of the reliability of the classifications. Chen et al. [50] propose a forecasting model based on RF, including the evaluation of a confidence interval based on an ensemble forecast provided to cover nearly all observations reasonably well, except for a few extreme drought events. In [51] the approach is very similar to the previous one, and exploits a Monte Carlo simulation to generate multiple datasets, training multiple RF structures and modeling the uncertainties of the classification from the variability of the results. Another work [52] provides a very detailed analysis on the topic of uncertainty in RF classification, and demonstrates that formal statistical inference procedures are possible within the context of supervised learning, even when individual base learners are difficult to analyze mathematically. With respect to this last work, the Sigma-z RF approach introduces an important element related to the assessment of classification uncertainty: the influence of the uncertainty of the feature entry as a physical measurement.

To the best of our knowledge, there are no other approaches like the one proposed in this paper.

III. Setup

In our system, the gait phase measurements are performed using a pair of forearm instrumented crutches, previously developed by our research group and described in [53].

The instrumented crutches are equipped with a set of four 350 Ω strain gauges to measure the axial force exerted by the user. The measurement recording and transmission are wireless, thanks to a low-energy Bluetooth device mounted directly on each crutch.

The instrumented crutches have been modified mounting a *Camboard Picoflexx* (PMD Technologies®) TOF camera on each crutch. The camera has a resolution of 224 x 171 pixels and a field of view of 62° x 45°. The depth measurement range spans from 0.01 to 0.4 m, with a frame rate within 5 and 45 fps. In the performed experiments, the camera frame rate was set to 14 fps.

The camera is very small (dimensions are 68 x 17 x 7.25 mm^3) and lightweight (8 g) because it contains only the depth sensor. The camera is powered through a USB 2.0/3.0 interface and does not requires any other power supply. The USB interface is also used for data transmission. The metrological performances of the Picoflexx camera have been evaluated in [54]: even if the camera shows average performances in terms of measurement accuracy, it performs better than other TOF cameras (such as the Kinect V2) in terms of dependency on external infrared light noise sources. This makes the selected camera a good choice in wearable applications, especially for outdoor environments.

The cameras are mounted on the crutches in a position that maximizes the visibility of the controlateral foot (i.e., the camera mounted on the left crutch views the right foot and viceversa). The data acquisition and recording are performed using Raspberry PI 3 boards mounted on each crutch. The cameras are connected to the Raspberry boards using USB links. Image acquisition is performed using ROS packages. The acquired depth images are then sent to a client PC for subsequent elaboration. Figure 1 shows the configuration of the crutches, which are completely wireless to maximize the comfort of the user.

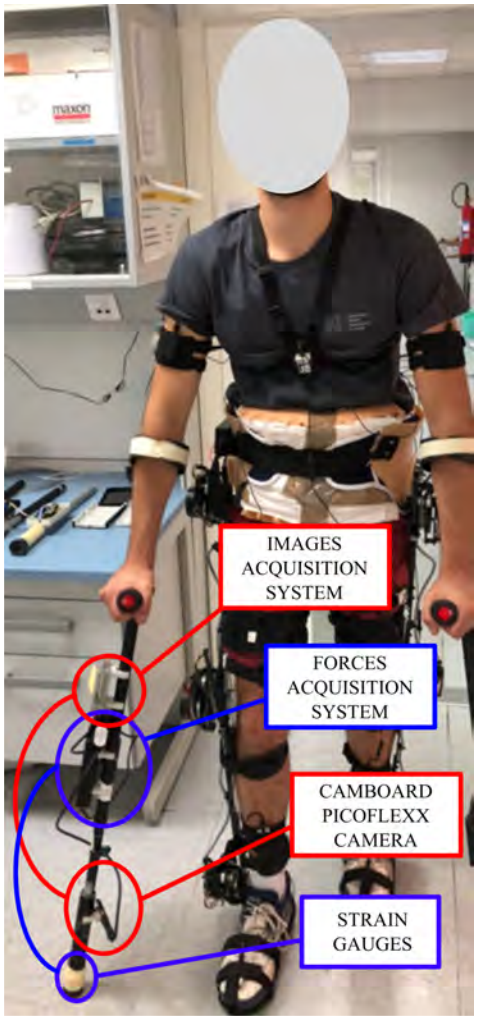

Figure 1: New version of instrumented crutches. Both the force and image acquisition systems are visible.

Figure 2 shows a sample image of the field of view acquired by the right camera during a swing phase: the left foot of the user is completely visible together with the floor and the environment. In the walking sessions the user performed an alternate gait (left foot and right crutch forwards, right foot and left crutch backwards, and viceversa), and the feet resulted always inside camera field of views.

IV. Method

The proposed analysis exploits two steps: 1) data collection and processing to extract the features' values from each acquired frame; 2) the assessment of features' uncertainties and classification.

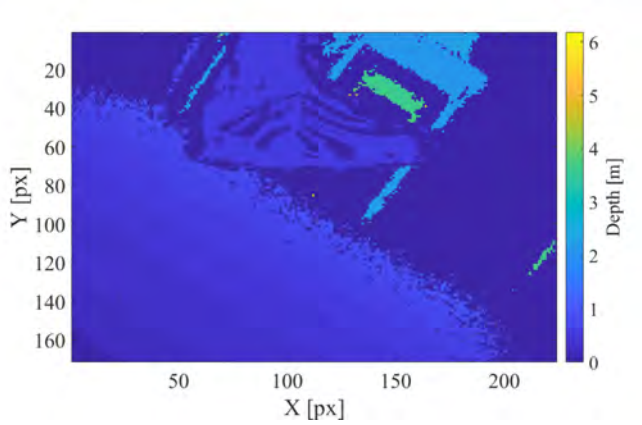

Figure 2: Example of the depth image of the left foot acquired with the right side camera.

A. Feature extraction

The features have been obtained from each frame in five steps: *(i)* a filter based on depth information is used to remove the environment, *(ii)* the floor is assessed using a plane detection algorithm, *(iii)* the distances between the floor and points not belonging to it are computed, *(iv)* the statistical features are extracted from these distances along with *(v)* their uncertainties.

In the first step, each frame is filtered in depth: only pixels with a depth value between D_{min} and D_{max} are maintained. The filter is used to remove the environment from the depth image. Figure 3a shows the result of the filter applied to the image of Figure 2; since D_{min} and D_{max} depend on the walking pattern of the subjects, they were set manually for each subject. These values were obtained experimentally and tuned to retain just the user's foot and the floor.

In the second step, a plane detection algorithm is applied to the resulting image, to discriminate between points belonging to the floor and points belonging to the foot. The well known iterative RANSAC algorithm is used [55] to fit a plane containing the majority of the measured points. The points are then divided into points laying on this plane (the inlier points, on the floor), and the others (the outlier points). Figure 3b shows an example of the algorithm results, displaying in red the plane detected from the image of Figure 3a. The inlier points are used to assess the parameters of the plane defining the floor, while the outlier points are assumed to belong to the foot.

In the third step, the distances between the floor plane and the points belonging to the foot are computed, ad their cumulative distribution is formed. As an example, Figure 3c shows the cumulative distribution of the distances computed from points of Figure 3b. The values of the cumulative distribution of the distances depends on the foot state: during stance the distances are small, during swing they assume higher values.

In the last step, a number of percentiles are extracted from the cumulative distances dataset, using the Matlab® *prctile* function. These values are used as predictors of the classification model. To take advantage of the chronological sequence of the recorded frames, each i^{th} set of features is composed of the percentiles of either the i^{th}, the $(i-1)^{th}$ frame, and the $(i-2)^{th}$ frames.

To understand which percentiles select as features, a preliminary gait test has been conducted, recorded and analyzed. An iterative procedure was used to identify the minimum number of percentiles needed to train the classification model. In the first iteration the 1^{st}, the 99^{th} and all the multiple of the 5^{th} percentiles have been computed for each frame of the analyzed gait. Then, the correlation matrix between the values of each pair of considered percentiles during the whole gait test has been computed. Subsequently, we progressively reduced the number of considered percentiles by removing the element of the couple with the highest correlation; then we computed the new correlation matrix. This step was repeated until each element of the correlation matrix was lower than 95%. At the end of this iterative procedure, the minimum set of percentiles was composed of the 5^{th}, the 25^{th}, the 50^{th}, the 75^{th}, and the 95^{th} percentiles. These five values have been computed for each frame of the acquired gaits. They are plotted in Figure 3c (dotted red lines).

The resulting set of features is as follows:

- The 5^{th}, the 25^{th}, the 50^{th}, the 75^{th}, and the 95^{th} percentiles computed on the i^{th} frame;
- The 5^{th}, the 25^{th}, the 50^{th}, the 75^{th}, and the 95^{th} percentiles computed on the $(i-1)^{th}$ frame;
- The 5^{th}, the 25^{th}, the 50^{th}, the 75^{th}, and the 95^{th} percentiles computed on the $(i-2)^{th}$ frame.

As a result, 15 features are used to train the classification model.

B. Sigma-z Random Forest classification algorithm

The Random Forest (RF) model is the result of the combination of multiple detection trees (*DTs*), identified from a subset of suitable features in the training set, through a bootstrapping operation [12], [56], [57]. A DT is a logic structure consisting of several nodes, each with one incoming branch and two branches departing from it. At each *n-th* node, a specific feature f_m and a threshold value $T_{n,m}$ of that feature are considered in the decision process that connects the node to a deeper level of the structure. Both the feature and the threshold are identified in the training phase and vary from tree to tree. The standard classification approach uses a binary threshold-based criterion: $f_m \leq T_{n,m}$. Depending on the outcome of the logic operation, the decision is then moved to one of the two possible deeper nodes, omitting the remaining part of the structure from the process. This logic continues until an end-node of the DT structure is reached: a leaf associated with a class *C*. The results of the complete RF model foresee the combination of all trees as independent concurrent constituting elements for the classification.

The Sigma-z RF algorithm leaves the original RF classification structure untouched, but considers *(i)* the uncertainty of the measured data, and *(ii)* the uncertainty deriving from the intrinsic variability of data in a class, i.e., the variance of data samples. The former is caused either by errors in the measurement process or in the propagation of uncertainty

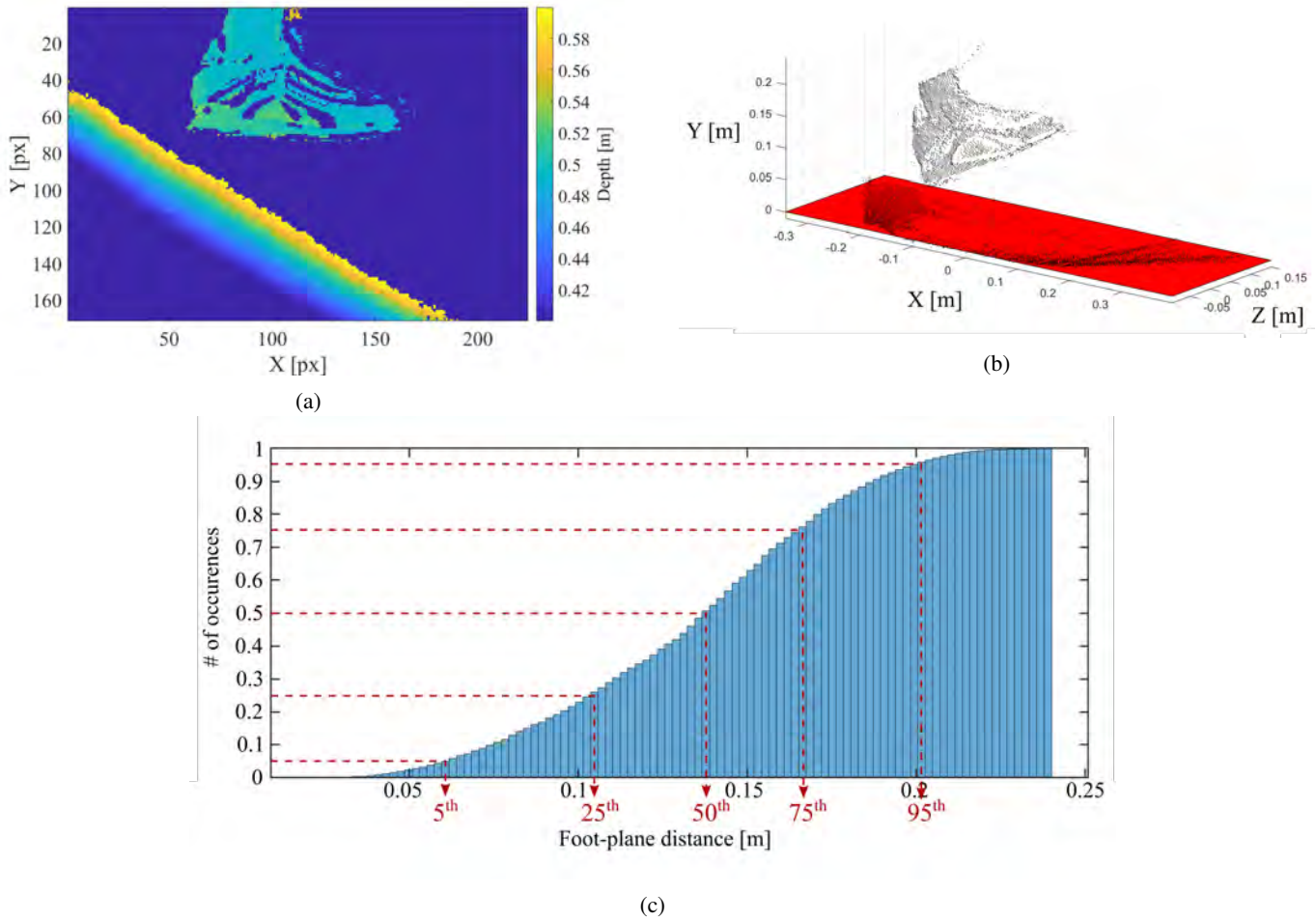

Figure 3: Image processing for features extraction: (a) depth filter; (b) plane detection; (c) computation of cumulative distribution of distances and percentiles extraction.

down to the evaluation of the feature; the latter depends on the distribution of the classes, and become relevant when the classes are similar, and the distribution of features from different classes overlap [13]. The *"sigma"* component of the algorithm accounts for the uncertainty associated with new input entries, the *"z"* component relates to the statistics used in the analysis of the input with respect to the training set.

1) The "sigma" component of the Sigma-z RF algorithm: This part of the algorithm is designed to include the uncertainty of the input features as a modifying factor in the splitting criterion. The uncertainty of the features is expressed by the standard deviation σ_m of their distribution, supposing it a Gaussian distribution.

At each node of the DT, the probability density function *PDF(x, σ_m)* of the distribution of feature f_m is computed and the two quantities expressed in (1) are obtained:

$$P_L^* = \int_{-\infty}^{T_{n,m}} PDF(x, \sigma_m)$$
$$P_H^* = \int_{-T_{n,m}}^{+\infty} PDF(x, \sigma_m). \quad (1)$$

Probabilities P_L^* and P_H^*, represent the level of reliability that the feature value f_m comes from distribution values lower (P_L^*) or higher (P_H^*) than the threshold node value $T_{n,m}$.

The values calculated in (1) are propagated through the next level of the DT as in (2):

$$P_L^b = P^{b-1} * P_L^*$$
$$P_H^b = P^{b-1} * P_H^*. \quad (2)$$

In (2), b is the level of the node, P^{b-1} is the probability value associated to the branch coming from the node at level (*b-1*), and P_L^b and P_H^b are the probability values flowing in the L/H branches departing from the node at level b. The process is recursive: at level $b = 0$, P^0 is set to 1, for normalization; at each iteration, (1) and (2) are used, and P^{b-1} is set to either P_L^b or P_H^b depending on the side of the splitting.

Remember that the DT is learned through training and is already optimized to achieve the best classification performance; hence, values calculated in (1) are propagated in the DT as node independent probabilities, which do not alter the splitting criterion of each node. The effect of this is that the information content can be interpreted as flowing and subdividing through

successive nodes of the DT, giving more relevance to those branches that achieve an overall higher node probability in the decision process. The process is repeated through all the nodes of the DT, until all leaves are reached. In the case of a leaf node *l*, the probability P^{b-1} becomes the probability $P^l_{C_i}$ of class C_i at that leaf. All $P^l_{C_i}$ are then summed for each class, forming a vector of probabilities P_{C_i} that indicates which class presents the highest probability of being the correct one. It holds that $\sum_i P_{C_i} = 1$.

In this approach, the entire structure of the tree is used, following the idea that all constitutive elements play an active role in the classification, each one probabilistically weighted. Features values f_m very close to the node threshold $T_{n,m}$ result in probabilities P^b_L and P^b_H around 50% and assign the same importance to both branches departing from the node. This means that both the branches present a low reliability of the choice, which is compliant with the fact that the feature value is close to the splitting criterion, just as a result of small fluctuations in the measurements. At each leaf node, value P_{C_i} give information about the confidence level of the classification, i.e expresses the probability that class C_i does not get confused with other classes.

In our application, the classifier provides two classes, corresponding to the swing and to the stance gait phases, and two confidence levels, one for each class. These represent independent estimators of the reliability in choosing that class as final result, independently from the other (the probabilities do not complement to one). The features extracted in correspondence to the stance and to the swing present values far from the splitting criterion at each node, and result in different reliability values propagating in the two output branches. Hence, the classification is made looking at the class with the highest confidence P_{C_i}. Instead, those features coming from the stance-swing transition are affected by a high uncertainty, and are close to the splitting criterion; in this case, the confidence levels that propagate in the branches are around 50%: the reliability of their classification as swing or stance is very low, and the frames are considered *unclassifiable*.

In examining the test gait sequence, the expected behavior is then a synchronous fluctuation of the confidence values P_{C_i} during the stance and swing phases, with the two values close to 50% during the transition of the gait phase.

2) Assessment of the uncertainty of the features: For a given feature f_m, a Monte Carlo simulation was run to obtain the value σ_m. Following the approach implemented in [58], the measurement noise of the point clouds resulting from the TOF cameras has been considered zero-mean, normally distributed. For each frame, 30.000 new point clouds were obtained, moving each single measured point in the 3D space by a random quantity following a normal distribution centered in zero, with standard deviation σ_{TOF} of 2 mm, as suggested in [54]. Since no prior information on the relative position of the cameras, the feet and the ground is assumed, the value of σ_{TOF} was supposed equal for all directions. The outcome for each frame is represented by 30.000 feature sets $F = [f_1, f_2, ..., f_m, ..., f_{15}]$: the standard deviation among the distribution of each feature f_m is then computed, resulting in the value σ_m, which is representative of the uncertainty of that feature, for that frame. The features and the associated uncertainties are then passed to the Sigma-z RF model, frame by frame.

3) The "z" component of the Sigma-z RF algorithm: This part of the algorithm focuses on the evaluation of the probability that a new datum belongs to a given population of known expected value and variance. The algorithm is as follows: *(i)* in the training data, the distributions of the 15 feature values are considered for each class and the mean value μ and the variance S are calculated and used to model each distribution as a normal distribution; *(ii)* the features values of a new input frame are then z-tested with all the distributions calculated in *(iii)* and the probability $p_{m,i}$ that feature f_m belongs to class C_i is kept, generating a matrix of 15 x 2 values. Note that, since each value $p_{m,i}$ estimates the probability that feature f_m belongs to class C_i or not, independently of the other class, the sum of values $p_{m,i}$ in a row over the 2 columns is not required to be equal to 1. These probability values can then be seen as independent forecasters on the origin of the data, and can be combined as follows [59]:

$$P_i = \frac{\left[\prod_{m=1}^{M}\left(\frac{p_{m,i}}{1-p_{m,i}}\right)^{w_m}\right]^a}{1+\left[\prod_{m=1}^{M}\left(\frac{p_{m,i}}{1-p_{m,i}}\right)^{w_m}\right]^a} \tag{3}$$

In (3), *a* represents the confidence of the forecaster (set to 1 to address the maximum confidence), and P_i is the result of the combination for the 15 features. Parameter w_m is a weighting factor. Values w_m are assessed during the training phase and represents the influence of each feature in the classification process.

4) Combination of "sigma" and "z" contributions: The last step of the algorithm foresees the combination of the two contributions, i.e. P_{C_i} and P_i, first within each single tree DT, and then for the entire forest. Since all the probabilities computed so far represent independent estimates, they can be combined using the same notation used in (3), this time with a uniform weighting factor equal to 50% for the sample related and the population related contributions, and equal to $1/N_t$ for the forest, giving the same importance to all N_t DTs. The result is a vector P of two values P_{Stance} and P_{Swing} representing the confidence associated to each class given the input feature entry: the highest value corresponds to the most reliable solution of the considered classification problem.

An *"admittance"* threshold T is introduced to define unclassifiable frames, which are characterized by values P_{Stance} and P_{Swing} lower than T.

V. Experimental results

A. Experimental protocol

The classification algorithm was validated classifying the gaits performed by four users (called A, B, C, and D respectively) wearing a Rewalk™ exoskeleton (Argo Medical Technologies Ltd., Yokneam Ilit, Israel). All participants gave informed consent. Gaits were performed both indoor, at the gym of the "Domus Salutis" Hospital in Brescia [60], and in three different outdoor environments (paved road, concrete

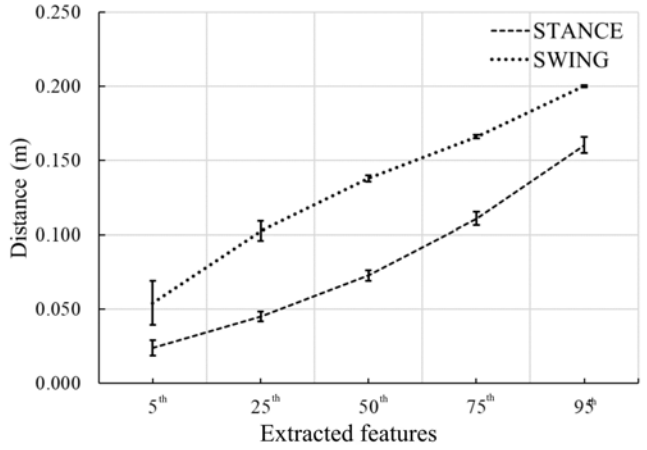

Figure 4: Results of the Monte Carlo simulations for a frame of test number 1 recorded during swing (dotted line) and one during stance (dashed line). Average values (lines) and sigma (error bars) of percentiles are shown

.

yard, and marble floor) along straight paths. Each user was preliminary trained to the use of the exoskeleton. Table I shows the characteristics of each analyzed gait. Seven tests have been conducted. For each test, the user performed two gaits: the former to train the classification algorithm, the latter to classify the gait phases using the trained model. Each frame of the training set was manually analyzed and labeled to identify the actual gait phase: stance and swing frames were labeled with the numerical identifiers "1" and "2" respectively, invalid frames were labeled with "0".

As stated before, values D_{min} and D_{max} used in the depth filtering step of the algorithm depend to the walking pattern of the subjects and were tuned experimentally for each subject. The chosen values are shown in Table II.

B. Classification results

We firstly analyzed the quality of the features extracted from each frame. An example of the analysis is shown in Figure 4 for two different frames of test number 1: one taken during swing (dot line), the other during stance (dashed line). The standard deviations σ_m computed using the Monte Carlo analysis spanned the range from 3.3 mm to 5.6 mm (4.5% and 7.7% of the median value) in the case of frames captured during stance, and from 0.7 mm to 15 mm (0.5% and 10% of the median value) in the case of frames captured during swing. The results show that standard deviations present higher values for frames taken during swing than during stance. The stance line is well separated from the swing line, i.e. the features obtained in the stance frame are significantly different from those obtained during the swing frame. Similar results have been obtained for every test. This result shows that the chosen feature set is appropriate for the classification algorithm.

The performances of the proposed classification algorithm have been assessed computing the classification accuracy, defined as the ratio between the number of correct predictions and the number of analyzed frames, using (*i*) the standard RF algorithm [61], and (*ii*) the Sigma-z RF algorithm with an admittance threshold T equal to 50%. Setting the admittance threshold to this value results in considering unclassifiable those frames presenting P_{Stance} and P_{Swing} less than 50%. Obviously, this increases the average classification accuracy. Table III shows the accuracy obtained in the experimental tests using the standard RF algorithm (*Standard RF* column), and using the Sigma-z RF algorithm (*Sigma-z RF* column). In addition, the difference between them (Δ *accuracy* column) and the number of unclassifiable samples obtained (last column) are reported.

Table III shows that in every test, classification accuracies obtained from Sigma-z RF algorithm increase. It is evident that those frames misclassified by the standard RF algorithm actually corresponds to unclassifiable frames in the Sigma-z RF algorithm. The average accuracy increment is equal to 4.3%. The Sigma-z RF algorithm detects a lower number of unclassifiable samples (average value equal to 4% of analyzed frames). This result is acceptable for gait analysis applications.

As an example, Figure 5 reports the gait sequence and the classified phases as a function of number of samples, obtained in test number 1 using the standard RF algorithm; in this case, no confidence values are returned. Black dots represent the i-th frame, blue circles represent the classification outputs (stance or swing), and red crosses represent the misclassified frames. As can be noticed from the distribution of the misclassified frames, as expected, these are mainly located in proximity of a transition gait phase. On the other side, the frames coming from the stable part of the gait are correctly classified. This behavior underlines the limitation of the standard RF model, which tends to provide erroneous classification outcomes in correspondence to the most critical events, i.e. the transitions.

Figure 6a shows the confidence obtained for the same test of Figure 5 using the Sigma-z RF classifier, as a function of analyzed samples. Here, it is visible the oscillatory behavior of values P_{Stance} and P_{Swing} between stance and swing phases: when a transition occurs, the two values intersect at about 50% as expected.

Figure 6b reports the results obtained with the Sigma-z RF classifier in test number 1. As before, black dots represent the i-th frame, blue circles represent the classification outputs (stance or swing), and red crosses represent misclassified frames. Unclassified frames are represented as black circles. Unclassified frames occur periodically in correspondence of a transition between stance and swing. These frames have been excluded from the classification and, thus, represent a loss of data. In this test, the unclassified frames are 22, equal to the 6.6% of the acquired frames. Similar results were obtained in every test.

C. Optimization

The admittance threshold T is a parameter that influences the behavior of the classifier: a low value (close to the theoretical minimum of 50%) provides a dense (several frame in time) but less reliable classification; a high threshold causes instead the rejection of the *uncertain* samples (and thus a lower frequency in the classification output) but a higher accuracy

Test number	Subject ID	Environment	Gait number	Duration [s]	Number of frames
1	A	Indoor	1 (training)	287.4	2801
			2 (classification)	34.5	333
2	B	Indoor	1 (training)	159.7	1555
			2 (classification)	29.4	285
3	B	Outdoor (concrete yard)	1 (training)	149.5	1454
			2 (classification)	63.8	613
4	C	Indoor	1 (training)	511.8	4973
			2 (classification)	100.3	963
5	C	Outdoor (marble floor)	1 (training)	431.4	4201
			2 (classification)	108.9	1045
6	D	Indoor	1 (training)	333.6	3242
			2 (classification)	75.5	723
7	D	Outdoor (paved road)	1 (training)	319.8	3106
			2 (classification)	54.4	522

Table I: Characteristics of the analyzed gaits.

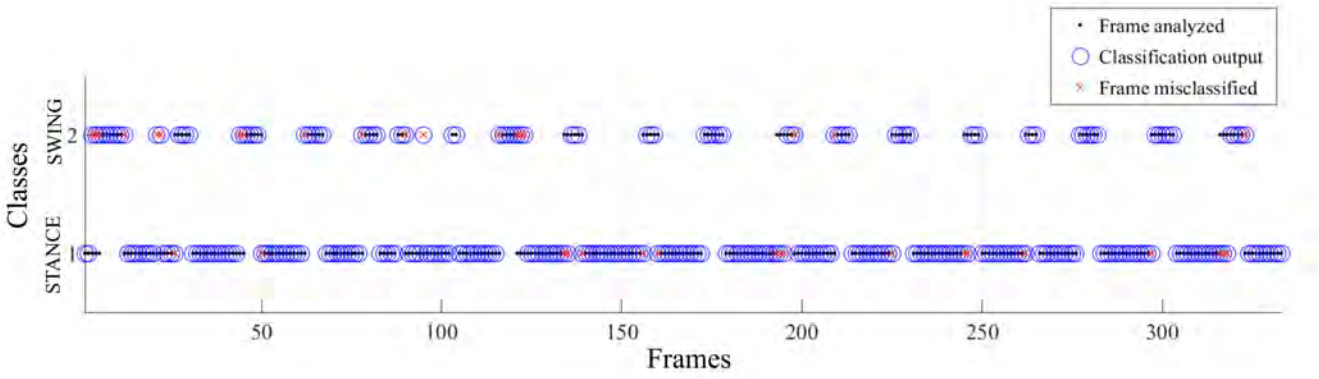

Figure 5: Classification results obtained with the standard version of the Random Forest algorithm in test number 1. Classification accuracy = 88%.

Subject ID	D_{min} [m]	D_{max} [m]
A	0.40	0.60
B	0.33	0.55
C	0.31	0.57
D	0.29	0.67

Table II: Values D_{min} and D_{max} chosen for each subject.

Test number	Standard RF	Sigma-z RF	Δ accuracy	Unclaffiable samples (% of analyzed frames)
1	88%	92%	+4%	22 (6.6%)
2	81%	84%	+3%	9 (3.2%)
3	79%	84%	+6%	25 (4.1%)
4	79%	83%	+4%	9 (0.9%)
5	76%	78%	+2%	7 (0.7%)
6	86%	91%	+5%	78 (10.8%)
7	78%	85%	+7%	8 (1.5%)
Average value	81%	85.3%	+4.4%	4%

Table III: Classification results obtained with standard RF and Sigma-z RF algorithms.

is expected. The trade-off comes from the magnitude of the sample loss resulting from the rejection, with a consequent reduction in the update rate of the system, despite these outputs result more reliable.

This effect has been analyzed running the Sigma-z RF algorithm by varying the admittance threshold T and computing the average classification accuracy and the percentage of the total classifiable samples.

As an example, Figure 7 reports the results of such comparison for test number 1 (compatible behavior have been obtained for every test).

As expected, the increase of the confidence threshold leads to higher accuracy but also to a higher amount of unclassifiable samples.

Such analysis can be used to optimize the admittance threshold T. Different strategies could be applied to choose the optimal admittance threshold *T**, relying either on the minimum admissible accuracy or on the maximum number of unclassifiable samples. In our experiments, we chose T* as the value that allows the system to maintain at least the 85% of the total number of samples. In Figure 7, for example, this value correspond to T*=57%: in this condition in fact, the system maintains the 85% of the total samples, and the average classification accuracy is higher than 90%. Table IV shows the values of the optimal threshold *T** obtained for all the considered test.

Test number	1	2	3	4	5	6	7
T*	57%	63%	59%	72%	78%	53%	64%

Table IV: Values of optimal admittance threshold T* obtained.

These values have been used in the *optimized* version of

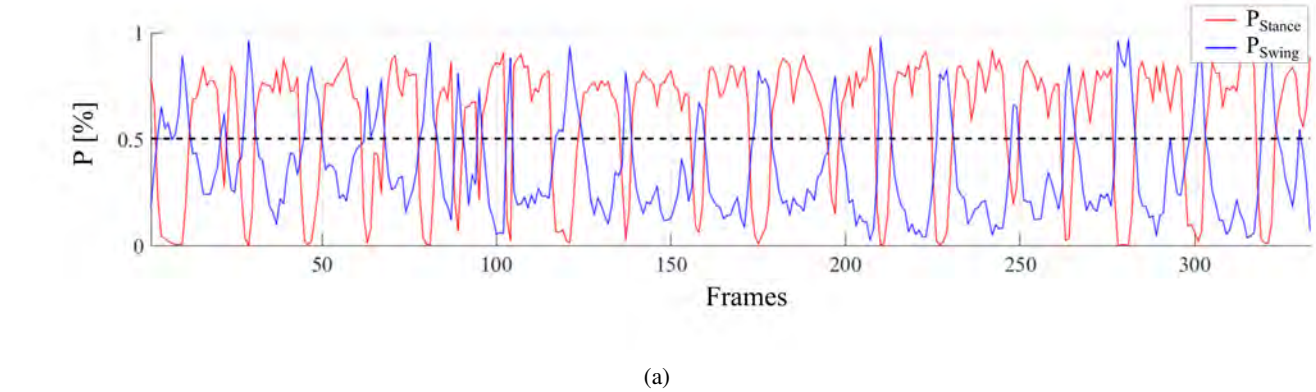

(a)

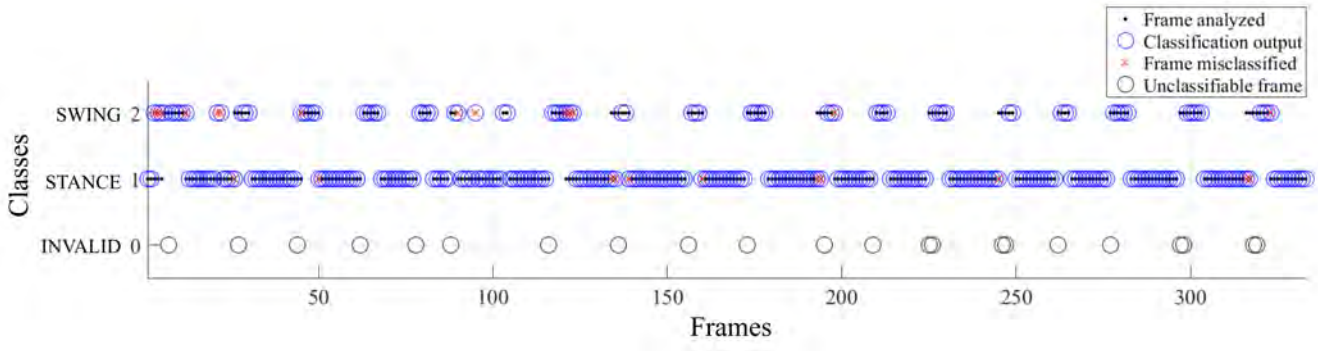

(b)

Figure 6: Classification results obtained using the Sigma-z Random Forest algorithm for test number 1, admittance threshold T equal to 50%, accuracy equal to 92%. (a) confidence P of both classes: swing (1) and stance (2). (b) identified classes, classification output, mis-classified and unclassifiables frames.

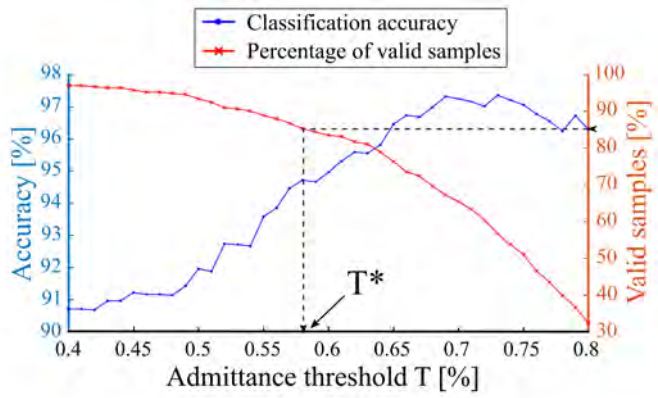

Figure 7: Comparison of classification accuracy and percentage of valid samples versus the admittance threshold T on the confidence probability for test number 1. A higher threshold lowers the number of *valid* samples but increases the overall accuracy and reliability of the classification. T* represents the optimal admittance threshold used in our experiments.

Test number	Sigma-z RF (T=T*)	Unclassiffiable samples (% of analyzed frames)	Δ accuracy standard RF	Δ accuracy (Sigma-z RF, T=50%)
1	94%	44 (13.2%)	+6%	+2%
2	86%	40 (14%)	+5%	+2%
3	87%	89 (14.5%)	+8%	+3%
4	85%	143 (14.9%)	+6%	+2%
5	80%	153 (14.6%)	+4%	+2%
6	92%	106 (14.7%)	+6%	+1%
7	87%	73 (14%)	+9%	+2%
Average value	87.3%	14.3%	6.3%	2%

Table V: Classification accuracy obtained with the optimized Sigma-z RF algorithm.

the Sigma-z RF algorithm. The classification results, together with the difference between the accuracies obtained before are reported in Table V.

The optimized Sigma-z RF algorithm reaches an average accuracy of 87.3%, and improves the performances of the standard RF algorithm of 6.3%. The optimized threshold T* leads to a further improvement of 2% with respect to the results obtained setting the admittance threshold T equal to 50%.

As an example, Figure 8 reports the gait sequence and the classified phases as a function of the number of samples obtained in test number 1, using the optimized version of the Sigma-z RF algorithm. The optimized solution outperformed the previous results. Figure 8 highlights the samples misclassified by the system. These are associated to a transition phase and usually are the last sample of a steady state. It

is worth nothing that this effect could be potentially related to minor discrepancies among the physical action and the labeling of the frame. As for the steady state, the results highlight good reliability in the identification of the gait phase, which represents a core functionality for the applicability of the method in the operative scenario. In the optimized version of the Sigma-z RF algorithm, we obtained 44 unclassifiable frames, equal to the 13.2% of the acquired frames. The sample loss is acceptable for our application. Similar results were obtained in every test.

Finally, as an example, Figure 9 shows the previously described results (test number 1) in the form of confusion matrices. The performances of the standard RF algorithm (Figure 9a), of the Sigma-z RF algorithm with T=50% (Figure 9b), and T=57% (optimized value, Figure 9c) are shown. All the matrices show that the classification errors are uniformly distributed into swing errors (i.e. stance frames classificated as swing) and stance errors (i.e. swing frames classificated as stance). This result confirms that the misclassified frames are associated to transitions between the gait phases. The amount of correctly classified frames remains nearly the same within the three cases. This confirms that the Sigma-z RF algorithm removes frames which are erroneously classified by the standard RF algorithm.

The ability of the Sigma-z RF algorithm to detect the gait phases was analyzed comparing nominal and measured heel strike and toe off contacts. Table VI shows the results in terms of the absolute difference (number of samples) between nominal and measured heel strike and toe off. As expected, the differences increase in the Sigma-z RF case. This confirms that the proposed algorithm marks as unclassifiable the frames closer to transitions between stance and swing, while it correctly predicts frames during steady states. The performances in contacts detection are linearly dependent on the quality of the phases prediction: lower performances (higher differences) were obtained in tests number 4 and 5, (relative both to subject B), which are those with the lower accuracy. These results are probably due to the quality of gaits performed by subject B, rather than to the classification algorithms.

VI. Conclusion

This paper presents a classification method for gait analysis in the context of assisted walking through power gait orthosis. The method is based on the frame by frame analysis of a sequence of depth images collected from a miniaturized depth camera attached at the bottom part of a pair of instrumented crutches used for the gait.

The depth images acquired by each camera deliver the point cloud of the controlateral foot, of the floor and of the background captured in the field of view. Suitable image preprocessing is carried out *(i)* to segment the foot and the ground from the background, *(ii)* to segment the foot from the ground, and *(iii)* to extract 5 features as the percentiles of the distances of the off-ground data from the ground. The feature set of each single frame is formed using the features extracted by the frame itself, plus the previous and the following frames, for a total of 15 features.

Gait classification focuses at detecting the stance and the swing phases. A novel approach, previously proposed by some of the authors, is adopted here: the algorithm is based on a Random Forest powered by the ability to account for the feature uncertainties. The method yields to the identification of each class with an associated confidence level, which enables the identification of potentially erroneous classification outcomes, usually associated to the transition among stance and swing.

The frames collected during this transition achieve a confidence usually lower, or close, to 50%. Such level can be interpreted as a random binomial outcome and thus as an index of low reliability of the classification for such samples.

The rejection of the samples marked by a confidence lower than a fixed admittance threshold dramatically improves the overall classification accuracy. A convergence analysis was run on the optimal threshold level, focusing on the trade-off between classification accuracy and the frame loss resulting from the frame rejection. In our experiments, we chose as the optimal threshold the value that allows the system to maintain at least the 85% of the analyzed samples. Higher accuracy can be achieved by further rising the threshold, at the expense of a severe reduction of potentially valid frames. The overall system reached the required specification for the tackled application.

In this work, the assessment of the uncertainty of the features has been performed using a Monte Carlo numerical simulation. The choice was motivated by the need of assessing the whole method. However, it is out of doubt that an analytic approach remains preferable over the numeric one, to enable a more suitable implementation of the algorithms for real-time embedded computation, directly on the crutches.

Acknowledgment

Authors would like to thank Domus Salutis (Brescia, Italy) LARIN Lab staff, for the assistance provided during measurements, as well as patients and therapists participating in this research.

References

[1] G. Onose, V. Cârdei, S. T. Crăciunoiu, V. Avramescu, I. Opris, M. A. Lebedev, and M. V. Constantinescu, "Mechatronic wearable exoskeletons for bionic bipedal standing and walking: A new synthetic approach," *Frontiers in Neuroscience*, vol. 10, p. 343, 2016.

[2] J. L. Contreras-Vidal, N. A. Bhagat, J. Brantley, J. G. Cruz-Garza, Y. He, Q. Manley, S. Nakagome, K. Nathan, S. H. Tan, F. Zhu, and J. L. Pons, "Powered exoskeletons for bipedal locomotion after spinal cord injury," *Journal of Neural Engineering*, vol. 13, no. 3, p. 031001, apr 2016.

[3] A. Esquenazi, M. Talaty, A. Packel, and M. Saulino, "The rewalk powered exoskeleton to restore ambulatory function to individuals with thoracic-level motor-complete spinal cord injury," *American journal of physical medicine and rehabilitation*, vol. 91, pp. 911–21, 11 2012.

[4] S. Pérez-Nombela, A. del Ama, G. Prieto, E. Piñuela-Martín, V. Lozano-Berrio, D. Serrano-Munoz, A. Gil-Agudo, J. L. Pons, and J. Moreno, "Physiological evaluation of different control modes of lower limb robotic exoskeleton h2 in patients with incomplete spinal cord injury," *Biosystems and Biorobotics*, vol. 15, pp. 343–348, 10 2017.

[5] D. B Fineberg, P. Asselin, N. Harel, I. Agranova-Breyter, S. D Kornfeld, W. Bauman, and A. M Spungen, "Vertical ground reaction force-based analysis of powered exoskeleton-assisted walking in persons with motor-complete paraplegia," *The journal of spinal cord medicine*, vol. 36, pp. 313–321, 07 2013.

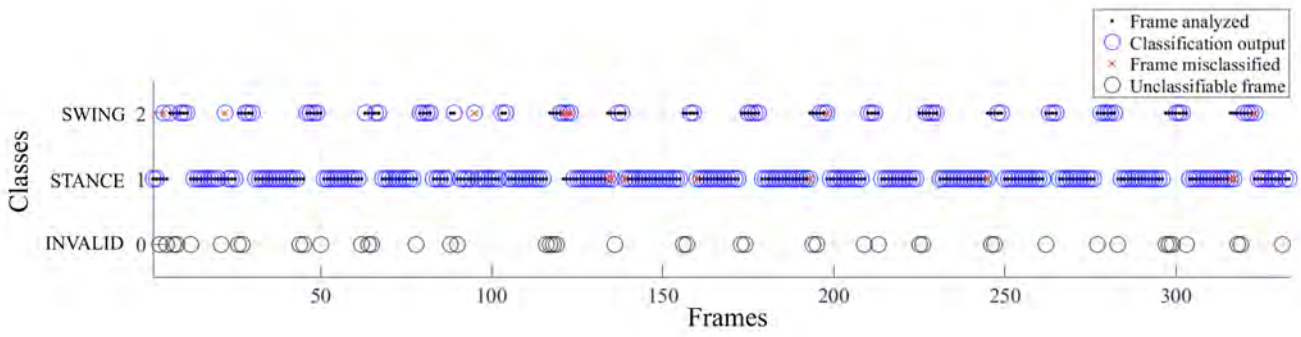

Figure 8: Classification results obtained with the optimized Sigma-z Random Forest algorithm in test number 1, admittance threshold on the confidence probability T* set to 57%. The accuracy equals 94%.

	Heel strike difference [frames]			Toe off difference [frames]		
Test number	Standard RF	Sigma-z RF (T = 50%)	Sigma-z RF (T = T*)	Standard RF	Sigma-z RF (T = 50%)	Sigma-z RF (T = T*)
1	1.05	1.47	1.79	0.56	0.50	0.56
2	1.15	1.60	1.60	0.84	0.58	0.63
3	1.33	1.37	1.60	0.79	0.74	1.07
4	1.22	2.15	5.12	1.54	1.49	3.85
5	1.68	3.46	11.41	1.56	5.29	14.63
6	1.27	2.22	2.34	1.00	1.48	1.53
7	1.37	1.43	2.17	0.84	0.78	1.47
Average value	1.30	1.96	3.72	1.02	1.55	3.39

Table VI: Comparison (in sample difference) between measured and nominal heel strike and toe off contacts, detected using standard RF and Sigma-z RF with T = 50%, and T = T*.

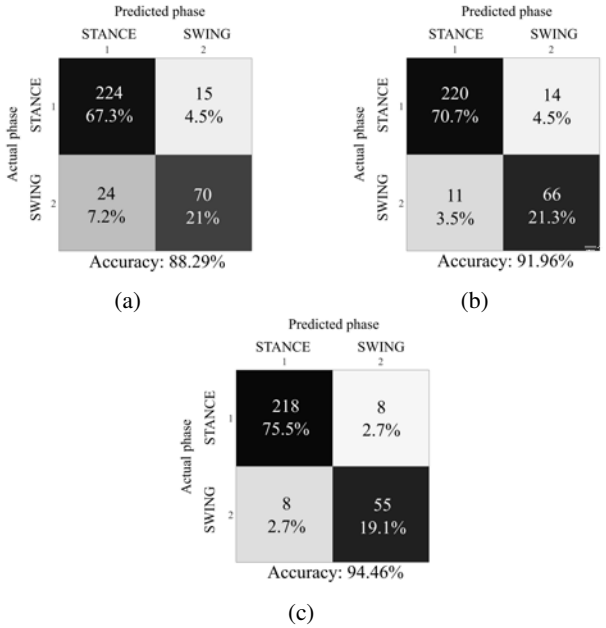

Figure 9: Confusion matrices of test number 1 with (a) the standard RF algorithm, and the Sigma-z RF algorithm with threshold T set to (b) 50% and (c) 57%.

[6] L. Lonini, N. Shawen, K. Scanlan, W. Z. Rymer, K. P. Kording, and A. Jayaraman, "Accelerometry-enabled measurement of walking performance with a robotic exoskeleton: a pilot study," *Journal of NeuroEngineering and Rehabilitation*, vol. 13, no. 1, p. 35, Mar 2016.

[7] M. T Alvarez, D. Torricelli, A. del Ama, D. Pinto, J. Gonzalez-Vargas, J. Moreno, A. Gil-Agudo, and J. L Pons, "Simultaneous estimation of human and exoskeleton motion: A simplified protocol," *IEEE International Conference on Rehabilitation Robotics : [proceedings]*, vol. 2017, pp. 1431–1436, 07 2017.

[8] M. Brodie, M. J M Coppens, S. Lord, N. Lovell, Y. Gschwind, S. Redmond, M. Del Rosario, K. Wang, D. Sturnieks, M. Persiani, and K. Delbaere, "Wearable pendant device monitoring using new wavelet-based methods shows daily life and laboratory gaits are different," *Medical and biological engineering and computing*, vol. 54, 08 2015.

[9] M. Lancini, M. Serpelloni, S. Pasinetti, and E. Guanziroli, "Healthcare sensor system exploiting instrumented crutches for force measurement during assisted gait of exoskeleton users," *IEEE Sensors Journal*, vol. 16, no. 23, pp. 8228–8237, 2016.

[10] M. Lancini, M. Serpelloni, and S. Pasinetti, "Instrumented crutches to measure the internal forces acting on upper limbs in powered exoskeleton users," in *Proceedings - 2015 6th IEEE International Workshop on Advances in Sensors and Interfaces, IWASI 2015*, 2015, pp. 175–180.

[11] E. Sardini, M. Serpelloni, M. Lancini, and S. Pasinetti, "Wireless instrumented crutches for force and tilt monitoring in lower limb rehabilitation," in *Procedia Engineering*, vol. 87, 2014, pp. 348–351.

[12] T. K. Ho, "Random decision forests," in *Proceedings of 3rd International Conference on Document Analysis and Recognition*, vol. 1, Aug. 1995, pp. 278–282 vol.1.

[13] A. Fornaser, M. De Cecco, P. Bosetti, T. Mizumoto, and K. Yasumoto, "Sigma-z random forest, classification and confidence," *Measurement Science and Technology*, vol. 30, no. 2, p. 025002, 2018.

[14] A. Zijlstra and W. Zijlstra, "Trunk-acceleration based assessment of gait parameters in older persons: A comparison of reliability and validity of four inverted pendulum based estimations," *Gait and Posture*, vol. 38, no. 4, pp. 940–944, 2013.

[15] C.-C. Yang, Y.-L. Hsu, K.-S. Shih, and J.-M. Lu, "Real-time gait cycle parameter recognition using a wearable accelerometry system," *Sensors*, vol. 11, no. 8, pp. 7314–7326, 2011.

[16] S. Yang, J.-T. Zhang, A. Novak, B. Brouwer, and Q. Li, "Estimation of spatio-temporal parameters for post-stroke hemiparetic gait using inertial sensors," *Gait and Posture*, vol. 37, no. 3, pp. 354–358, 2013.

[17] B. Mariani, H. Rouhani, X. Crevoisier, and K. Aminian, "Quantitative estimation of foot-flat and stance phase of gait using foot-worn inertial sensors," *Gait and Posture*, vol. 37, no. 2, pp. 229–234, 2013.

[18] S. Shahid, A. Nandy, S. Mondal, M. Ahamad, P. Chakraborty, and

G. Nandi, "A study on human gait analysis," in *ACM International Conference Proceeding Series*, 2012, pp. 358–364.

[19] D. Korotkin and K. Artem, "Inertial measurement system for human gait analysis," in *Proceedings of the 8th International Conference on Body Area Networks, BodyNets 2013*, 2013, pp. 414–419.

[20] S. Zhu, R. Ellis, G. Schlaug, Y. Ng, and Y. Wang, "Validating an iOS-based Rhythmic Auditory Cueing Evaluation (iRACE) for Parkinson's disease," in *MM 2014 - Proceedings of the 2014 ACM Conference on Multimedia*, 2014, pp. 487–496.

[21] B. Cole, S. Roy, C. De Luca, and S. Nawab, "Dynamic neural network detection of tremor and dyskinesia from wearable sensor data," in *2010 Annual International Conference of the IEEE Engineering in Medicine and Biology Society, EMBC'10*, 2010, pp. 6062–6065.

[22] W. Zhu, B. Anderson, S. Zhu, and Y. Wang, "A computer vision-based system for stride length estimation using a mobile phone camera," in *ASSETS 2016 - Proceedings of the 18th International ACM SIGACCESS Conference on Computers and Accessibility*, 2016, pp. 121–130.

[23] T. Moeslund, A. Hilton, and V. Krüger, "A survey of advances in vision-based human motion capture and analysis," *Computer Vision and Image Understanding*, vol. 104, no. 2-3 SPEC. ISS., pp. 90–126, 2006.

[24] S. Das Choudhury and T. Tjahjadi, "Silhouette-based gait recognition using Procrustes shape analysis and elliptic Fourier descriptors," *Pattern Recognition*, vol. 45, no. 9, pp. 3414–3426, 2012.

[25] E. Auvinet, F. Multon, and J. Meunier, "Lower limb movement asymmetry measurement with a depth camera," in *2012 Annual International Conference of the IEEE Engineering in Medicine and Biology Society*, 2012, pp. 6793–6796.

[26] E. E. Stone, D. Anderson, M. Skubic, and J. M. Keller, "Extracting footfalls from voxel data," in *2010 Annual International Conference of the IEEE Engineering in Medicine and Biology*, 2010, pp. 1119–1122.

[27] E. E. Stone and M. Skubic, "Passive in-home measurement of stride-to-stride gait variability comparing vision and Kinect sensing," in *2011 Annual International Conference of the IEEE Engineering in Medicine and Biology Society*, 2011, pp. 6491–6494.

[28] F. Caillette and T. Howard, "Real-time markerless human body tracking using colored voxels and 3d blobs," in *Third IEEE and ACM International Symposium on Mixed and Augmented Reality*, 2004, pp. 266–267.

[29] N. Biasi, F. Setti, A. Del Bue, M. Tavernini, M. Lunardelli, A. Fornaser, M. Da Lio, and M. De Cecco, "Garment-based motion capture (gamocap): high-density capture of human shape in motion," *Machine Vision and Applications*, vol. 26, no. 7-8, pp. 955–973, 2015.

[30] M. Derawi, H. Ali, and F. Cheikh, "Gait recognition using time-of-flight sensor," in *Lecture Notes in Informatics (LNI), Proceedings - Series of the Gesellschaft fur Informatik (GI)*, 2011, pp. 187–194.

[31] C. Altuntas, F. Turkmen, A. Ucar, and Y. Akgul, "Measurement and analysis of gait by using a time-of-flight camera," in *International Archives of the Photogrammetry, Remote Sensing and Spatial Information Sciences - ISPRS Archives*, vol. 41, 2016, pp. 459–464.

[32] R. Jensen, R. Paulsen, and R. Larsen, "Analysis of gait using a treadmill and a time-of-flight camera," *Lecture Notes in Computer Science (including subseries Lecture Notes in Artificial Intelligence and Lecture Notes in Bioinformatics)*, vol. 5742 LNCS, pp. 154–166, 2009.

[33] I. González, I. López-Nava, J. Fontecha, A. Muñoz-Meléndez, A. Pérez-SanPablo, and I. Quiñones-Urióstegui, "Comparison between passive vision-based system and a wearable inertial-based system for estimating temporal gait parameters related to the GAITRite electronic walkway," *Journal of Biomedical Informatics*, vol. 62, pp. 210–223, 2016.

[34] Y. Watanabe, T. Hatanaka, T. Komuro, and M. Ishikawa, "Human gait estimation using a wearable camera," in *2011 IEEE Workshop on Applications of Computer Vision, WACV 2011*, 2011, pp. 276–281.

[35] A. Kim, J. Kim, S. Rietdyk, and B. Ziaie, "A wearable smartphone-enabled camera-based system for gait assessment," *Gait and Posture*, vol. 42, no. 2, pp. 138–144, 2015.

[36] A. Catteau and M. Ahmadi, "Concept and preliminary experiments with a wearable computer vision system for measuring shoe position and orientation," *Measurement: Journal of the International Measurement Confederation*, vol. 75, pp. 273–283, 2015.

[37] B. Schneider and T. Banerjee, "Preliminary investigation of walking motion using a combination of image and signal processing," in *Proceedings - 2016 International Conference on Computational Science and Computational Intelligence, CSCI 2016*, 2017, pp. 641–646.

[38] J. Chee, W. Gage, W. McIlroy, and K. Zabjek, "Development of a video-based technique for ambulatory monitoring of foot placement with an instrumented rollator," *Journal of Rehabilitation Medicine*, vol. 47, no. 3, pp. 273–277, 2015.

[39] B. Sun, X. Liu, X. Wu, and H. Wang, "Human gait modeling and gait analysis based on Kinect," in *Proceedings - IEEE International Conference on Robotics and Automation*, 2014, pp. 3173–3178.

[40] C. Zong, P. Bidaud, and X. Clady, "A mobile 3d vision-based embedded system for robust estimation and analysis of human locomotion," in *Nature-Inspired Mobile Robotics: Proceedings of the 16th International Conference on Climbing and Walking Robots and the Support Technologies for Mobile Machines, CLAWAR 2013*, 2013, pp. 101–108.

[41] C. Wong, S. McKeague, J. Correa, J. Liu, and G.-Z. Yang, "Enhanced classification of abnormal gait using BSN and depth," in *Proceedings - BSN 2012: 9th International Workshop on Wearable and Implantable Body Sensor Networks*, 2012, pp. 166–171.

[42] V. Agostini, G. Balestra, and M. Knaflitz, "Segmentation and Classification of Gait Cycles," *IEEE Transactions on Neural Systems and Rehabilitation Engineering*, vol. 22, no. 5, pp. 946–952, sep 2014.

[43] S. Mohammed, A. Samé, L. Oukhellou, K. Kong, W. Huo, and Y. Amirat, "Recognition of gait cycle phases using wearable sensors," *Robotics and Autonomous Systems*, vol. 75, pp. 50–59, Jan. 2016.

[44] J.-Y. Jung, W. Heo, H. Yang, H. Park, J.-Y. Jung, W. Heo, H. Yang, and H. Park, "A Neural Network-Based Gait Phase Classification Method Using Sensors Equipped on Lower Limb Exoskeleton Robots," *Sensors*, vol. 15, no. 11, pp. 27 738–27 759, Oct. 2015.

[45] A. J. Young, A. M. Simon, N. P. Fey, and L. J. Hargrove, "Intent Recognition in a Powered Lower Limb Prosthesis Using Time History Information," *Annals of Biomedical Engineering*, vol. 42, no. 3, pp. 631–641, Mar. 2014.

[46] D.-X. Liu, X. Wu, W. Du, C. Wang, and T. Xu, "Gait Phase Recognition for Lower-Limb Exoskeleton with Only Joint Angular Sensors," *Sensors (Basel, Switzerland)*, vol. 16, no. 10, Sep. 2016.

[47] A. Thongsook, T. Nunthawarasilp, P. Kraypet, J. Lim, and N. Ruangpayoongsak, "C4.5 Decision Tree against Neural Network on Gait Phase Recognition for Lower Limp Exoskeleton," in *2019 First International Symposium on Instrumentation, Control, Artificial Intelligence, and Robotics (ICA-SYMP)*. IEEE, jan 2019, pp. 69–72.

[48] U. Martinez-Hernandez and A. A. Dehghani-Sanij, "Adaptive Bayesian inference system for recognition of walking activities and prediction of gait events using wearable sensors," *Neural Networks*, vol. 102, pp. 107–119, Jun. 2018.

[49] M. Ye, C. Yang, V. Stankovic, L. Stankovic, and S. Cheng, "Gait phase classification for in-home gait assessment," in *2017 IEEE International Conference on Multimedia and Expo (ICME)*. IEEE, jul 2017, pp. 1524–1529.

[50] J. Chen, M. Li, and W. Wang, "Statistical uncertainty estimation using random forests and its application to drought forecast," *Mathematical Problems in Engineering*, vol. 2012, 2012.

[51] J. W. Coulston, C. E. Blinn, V. A. Thomas, and R. H. Wynne, "Approximating prediction uncertainty for random forest regression models," *Photogrammetric Engineering & Remote Sensing*, vol. 82, no. 3, pp. 189–197, 2016.

[52] L. Mentch and G. Hooker, "Quantifying uncertainty in random forests via confidence intervals and hypothesis tests," *The Journal of Machine Learning Research*, vol. 17, no. 1, pp. 841–881, 2016.

[53] M. Lancini, S. Pasinetti, V. Montini, and G. Sansoni, "Monitoring upper limbs during exoskeleton-assisted gait outdoors," *Biosystems and Biorobotics*, vol. 22, pp. 127–131, 2019.

[54] S. Pasinetti, M. M. Hassan, J. Eberhardt, M. Lancini, F. Docchio, and G. Sansoni, "Performance analysis of the pmd camboard picoflexx time-of-flight camera for markerless motion capture applications," *IEEE Transactions on Instrumentation and Measurement*, vol. 68, no. 11, pp. 4456–4471, Nov. 2019.

[55] P. H. S. Torr and A. Zisserman, "MLESAC: A New Robust Estimator with Application to Estimating Image Geometry," *Computer Vision and Image Understanding*, vol. 78, no. 1, pp. 138–156, 2000.

[56] L. Breiman, *Classification and Regression Trees*. Routledge, Oct. 2017.

[57] T. K. Ho, "The random subspace method for constructing decision forests," *IEEE Transactions on Pattern Analysis and Machine Intelligence*, vol. 20, no. 8, pp. 832–844, Aug. 1998.

[58] M. Pauly, N. J. Mitra, and I. G. Leonidas, "Uncertainty and variability in point cloud surface data," in *Proceeding of the Eurographics Conference and Point-Based Graphics*, 2004, pp. 77–84.

[59] V. A. Satopää, J. Baron, D. P. Foster, B. A. Mellers, P. E. Tetlock, and L. H. Ungar, "Combining multiple probability predictions using a simple logit model," *International Journal of Forecasting*, vol. 30, no. 2, pp. 344–356, Apr. 2014.

[60] "Domus salutis homepage." [Online]. Available: http://www.domussalutis.it/,

[61] L. Breiman, "Random Forests," *Machine Learning*, vol. 45, no. 1, pp. 5–32, Oct. 2001.

Simone Pasinetti Simone Pasinetti received the B.S. degree and the M.S. degree (with honors) in Automation Engineering from University of Brescia, Brescia, Italy, in 2009 and 2011 respectively, with a thesis concerning the control of mechanical actuators with SEMG signals. He received the Ph. D. degree in applied mechanics from University of Brescia, Brescia, Italy, in 2015 with a thesis titled "Development of measurement protocols for the analysis of the functional evaluation and rehabilitation, in biomechanics field". During the Ph. D. he had in contact with the Institute of Intelligent Systems and Robotics (ISIR), Paris, France, where he carried out research concerning the dynamic posture analysis. Since January 2015, he has been a research fellow for the Laboratory of Vision Systems for Mechatronics (Vis4Mechs) in the Department of Mechanical and Industrial Engineering at University of Brescia, Brescia, Italy. He is currently working on posture and gait analysis, depth sensors, collaborative robotics, 2D and 3D vision systems development. His research interests include biomechanics of human posture, motion analysis, EMG analysis, collaborative robotics and 2D and 3D vision systems.

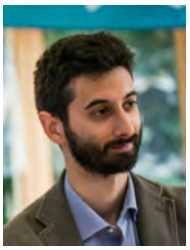

Alberto Fornaser Alberto Fornaser received the M.Eng. in mechatronic engineering from the University of Trento (Italy) in 2010, and his Ph.D. in Mechatronic Engineering at DICAM, Department of Civil, environmental and mechanical engineering in 2014, University of Trento. Co-Founder on the academic StartUp up Robosense srl. Research fellow at University of Trento, his research regards measurement systems for robotics, non-conventional measurements systems, data fusion, augmented reality, focusing in particular on low cost motion capture solutions and 3D data analysis.

Matteo Lancini Matteo Lancini received the master's degree in mechanical engineering in 2005 from the University of Brescia. He was a research contractor with the Department of Industrial and Mechanical Engineering, University of Brescia, Brescia, Italy, where he was involved in the development of measurement techniques for industrial diagnostics, and focused on measurements in uncontrolled environments from 2005 to 2009. He received his PhD degree in Applied Mechanics from the University of Brescia in 2015. He is currently an Assistant Professor with the Mechanical and Thermal Measurements Laboratory, Department of Industrial and Mechanical Engineering, University of Brescia. His current research interests include measurement systems for biomechanical analysis, in particular, for robotic gait and rehabilitation, and industrial diagnostics using nondestructive techniques based on vibration measurements. Dr. Lancini is a member of the International Society of Biomechanics.

Mariolino De Cecco Mariolino De Cecco Ph.D., associate Professor of Mechanical Measurements and Robotics at the University of Trento. Head of the MIRo (Measurement, Instrumentation and Robotics) laboratory (http://www.miro.ing.unitn.it/). Main fields of research are measurements, robotics and space. Participated as local responsible in the framework of international projects such as UNCAP H2020, VERITAS FP7 IP, AGILE Eurostars. Co. Investigator of OSIRIS payload of ROSETTA–ESA Cornerstone Mission. Participated to the LISA TEAM (LISA—ESA Cornerstone Mission). Co-proposer and member of the steering committee of the AUSILIA project. Co-founder of Robosense, University startup company. Referee of different international papers and congress, and of different national and international research projects. Author of more than 70 papers on international journal with referee, 1 book chapter, 39 papers on national or international congress with referee, H-index 20.

Giovanna Sansoni Prof. Giovanna Sansoni received her degree in Electronic Engineering at the Politecnico of Milan, Italy, in 1984. In 1985 she joined the University of Brescia, Italy. She is now Full Professor of Electrical Measurements at the Department of Mechanical and Industrial Engineering of the University of Brescia. Her main research interests are in the 3D vision area. Among these are the implementation of camera and projector calibration for the absolute measurement of shape in active stereo vision systems; the development of light coding methods for whole-field optical profilometry; the application of optical instrumentation to the acquisition and the reverse engineering of free-form surfaces. She is currently the head of the Laboratory of Visions Systems for Mechatronics at University of Brescia, Brescia, Italy.